Letter

Surrogate model solver for impurity-induced superconducting subgap states

Virgil V. Baran ,[1,2,3,4,*] Emil J. P. Frost ,[4,†] and Jens Paaske[4]

[1]*Research Institute of the University of Bucharest (ICUB), RO-050107 Bucharest, Romania*

[2]*Faculty of Physics, University of Bucharest, 405 Atomiştilor, RO-077125 Bucharest-Măgurele, Romania*

[3]*"Horia Hulubei" National Institute of Physics and Nuclear Engineering, 30 Reactorului, RO-077125 Bucharest-Măgurele, Romania*

[4]*Center for Quantum Devices, Niels Bohr Institute, University of Copenhagen, DK-2100 Copenhagen, Denmark*

(Received 29 July 2023; revised 19 October 2023; accepted 5 December 2023; published 20 December 2023)

A simple impurity solver is shown to capture impurity-induced superconducting subgap states in quantitative agreement with the numerical renormalization group and quantum Monte Carlo simulations. The solver is based on the exact diagonalization of a single-impurity Anderson model with discretized superconducting reservoirs including only a small number of effective levels. Their energies and couplings to the impurity d level are chosen so as to best reproduce the Matsubara frequency dependence of the hybridization function. We provide a number of critical benchmarks and demonstrate the solver's efficiency in combination with the reduced basis method [V. V. Baran and D. R. Nichita, Phys. Rev. B **107**, 144503 (2023)] by calculating the phase diagram for an interacting three-terminal junction.

DOI: 10.1103/PhysRevB.108.L220506

Introduction. Quantum dots (QD) tunnel-coupled to superconducting (SC) leads act as atomic Anderson impurities and induce Andreev bound states inside the superconducting gap. Depending on the parameters, these subgap states range from Yu-Shiba-Rusinov (YSR) states [1–3], induced by odd occupied Coulomb blockaded QDs with a local magnetic moment, to a localized quasiparticle excitation above an induced gap on proximitized QDs with a smaller charging energy [4–7]. These states are observed routinely either by scanning tunneling spectroscopy (STS) near adatomic Anderson impurities on superconductor surfaces [8–12], or in transport or microwave spectroscopy off semiconductor QDs contacted by superconductors [13–21]. Understanding their detailed behavior is therefore of great importance for interpreting detailed STS subgap spectra to infer about the host superconductor, as well as for the design of superconducting qubits and other complex gateable superconductor-semiconductor hybrid devices relying on engineered subgap states [21–24].

The bound subgap states induced by an Anderson impurity in a superconductor can be calculated within a number of different approximate methods, which correspond reasonably well with the numerically exact results of numerical renormalization group (NRG) or quantum Monte Carlo (QMC) (cf. Refs. [25–28] and references therein) calculations in different regions of parameter space. These include the original YSR approach neglecting spin flips [1–3,7,29], the infinite-gap (atomic) limit [5,29,30] and its recent generalizations [28,31], as well as the zero bandwidth (ZBW) approximation [32,33] of including only a single quasiparticle in the superconductor.

In contrast to the normal state, the finite BCS gap in the superconducting quasiparticle excitation spectrum Δ cuts off all logarithmic singularities and prevents an actual Kondo problem [34]. Unless its ratio to the Kondo temperature Δ/T_K is very small, the superconducting gap therefore saves a lot of calculational effort, leaving a simpler nonperturbative problem of solving for bound states inside the gap. In more technical terms, the finite gap ensures that the normal component of the local BCS Nambu Green's function, defining the tunneling self-energy $\Sigma_d^{\mathrm{T}}(\omega_n)$, vanishes linearly with the Matsubara frequency below the gap. This has the convenient consequence that the same Green's function can be readily obtained within a surrogate BCS model with a few discrete levels coupled to the d level (cf. Fig. 1). Here, we utilize this simplification to demonstrate that exact diagonalization (ED) of a low-dimensional surrogate BCS model coupled to the d level captures the numerically exact results obtained by NRG and QMC.

In the context of dynamical mean-field theory [35], ED has already been employed as an efficient impurity solver producing static thermodynamic quantities in very good agreement with QMC [36–39]. Within any finite-size approximation, however, one loses the ability to properly describe the spectral function of the continuum, which is reduced to a collection of δ peaks (cf., e.g., Fig. 18 of Ref. [35]). This limitation may be overcome by using an ensemble of discrete models within the so-called distributional exact diagonalization approach [40–42]. Whereas this could be relevant for a faithful description of the above-gap continuum, this Letter will focus exclusively on the discrete subgap states and corresponding equilibrium expectation values of various observables.

Model. We consider the superconducting Anderson impurity model Hamiltonian for a quantum dot (QD) coupled to a

*virgil.v.baran@unibuc.ro

†emiljpfrost@gmail.com

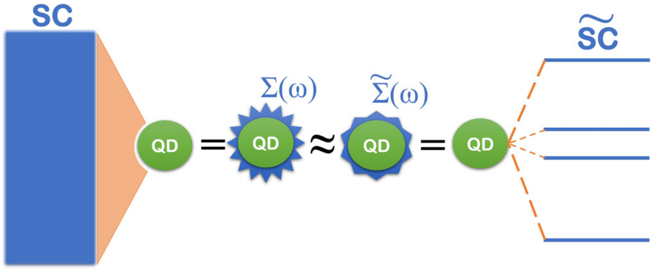

FIG. 1. Schematic of the surrogate model. SC lead (blue continuum) coupled to a QD (green) by a given hybridization strength (orange), giving rise to the tunneling self-energy $\Sigma_d^{\rm T}(\omega)$ of Eqs. (2) and (3) (blue spikes). This self-energy is approximated by the prescription of Eq. (4), corresponding to a few-level effective BCS model (blue $\widetilde{\rm SC}$), depicted here with $\tilde{L}=4$ particle-hole symmetric levels coupled to the QD by different pairs of tunneling amplitudes (dashed orange lines).

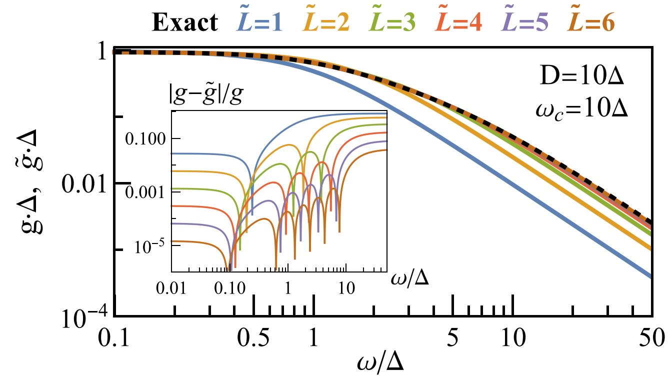

FIG. 2. The exact g function (3) (dashed black curve) and its best-fit approximations $\tilde{g}(\omega)$ (4) with $\tilde{L}\leqslant 6$. Inset: Relative errors for the same parameters.

single superconducting lead (SC),

$$\begin{aligned}
H &= H_{\rm QD} + H_{\rm SC} + H_{\rm T},\\
H_{\rm QD} &= \epsilon_d \sum_{\sigma=\uparrow\downarrow} d_\sigma^\dagger d_\sigma + U d_\uparrow^\dagger d_\uparrow d_\downarrow^\dagger d_\downarrow,\\
H_{\rm SC} &= \sum_{\mathbf{k}\sigma} \xi_{\mathbf{k}} c_{\mathbf{k}\sigma}^\dagger c_{\mathbf{k}\sigma} - \sum_{\mathbf{k}} (\Delta e^{i\varphi}\, c_{\mathbf{k}\uparrow}^\dagger c_{-\mathbf{k}\downarrow}^\dagger + \text{H.c.}),\\
H_{\rm T} &= \sum_{\mathbf{k}\sigma} (t c_{\mathbf{k}\sigma}^\dagger d_\sigma + \text{H.c.}). \qquad (1)
\end{aligned}$$

Here, $d_\sigma^\dagger$ creates an electron with spin σ and energy ϵ_d on the QD with a repulsive on-site Coulomb interaction U. Similarly, $c_{\mathbf{k}\sigma}^\dagger$ creates an electron with spin σ, momentum $\mathbf{k}$, and energy $\xi_{\mathbf{k}}$ in the SC lead with order parameter $\Delta e^{i\varphi}$, where Δ and φ are real numbers. The SC-QD tunnel coupling is described by $H_{\rm T}$, whose tunneling amplitudes t are taken to be momentum independent. We replace the momentum summation by an energy integral, assuming a constant density of states, $\nu_F = 1/(2D)$, in a band of half width D around the Fermi surface. The discussion below may be trivially generalized beyond these simplifying assumptions.

With the superconducting correlations being treated at the BCS mean-field level, the lead degrees of freedom are readily integrated out to give rise to the following Nambu tunneling self-energy (hybridization function) [4,5],

$$\Sigma_d^{\rm T}(\omega_n) = -\Gamma \begin{pmatrix} i\omega_n & \Delta e^{i\varphi} \\ \Delta e^{-i\varphi} & i\omega_n \end{pmatrix} g(\omega_n), \qquad (2)$$

with Matsubara frequencies $\omega_n = (2n+1)\pi k_{\rm B} T$ at temperature T, tunneling rate $\Gamma = \pi \nu_F |t|^2$, and the g function defined as

$$g(\omega) \equiv \frac{1}{\pi}\int_{-D}^{D} {\rm d}\xi \frac{1}{\xi^2+\Delta^2+\omega^2} = \frac{2}{\pi}\frac{\arctan\left(\frac{D}{\sqrt{\Delta^2+\omega^2}}\right)}{\sqrt{\Delta^2+\omega^2}}, \quad (3)$$

which will be our main interest for the discretization procedure outlined below.

Surrogate model. We are interested in constructing the simplest discrete effective bath that best reproduces the subgap states of the full model. For this purpose, we note that each SC level with energy ξ contributes a factor of $(\xi^2+\Delta^2+\omega^2)^{-1}$ to the g function (3). Therefore, we seek to approximate the latter by combining only a small number of such factors,

$$\begin{aligned}
\tilde{g}_{\rm even}(\omega) &\equiv 2\sum_{\ell=1}^{K} \frac{\gamma_\ell}{\tilde{\xi}_\ell^2+\Delta^2+\omega^2}, \quad \tilde{L}=2K,\\
\tilde{g}_{\rm odd}(\omega) &\equiv \frac{\gamma_0}{\Delta^2+\omega^2} + \tilde{g}_{\rm even}(\omega), \quad \tilde{L}=2K+1, \qquad (4)
\end{aligned}$$

where K denotes the number of pairs of effective levels. A $\tilde{g}$ function of this form may be obtained by integrating out an effective superconducting bath with the same gap Δ as the original one and whose $\tilde{L}$ discrete levels with energies $\pm|\tilde{\xi}_\ell|$ are coupled to the dot via a tunneling matrix element $\tilde{t}_\ell = \sqrt{\gamma_\ell \Gamma}$. Note that each odd-$\tilde{L}$ model involves one extra level at zero energy, $\tilde{\xi}_0 = 0$. The effective bath is thus defined by parameters $\{\gamma_\ell, \tilde{\xi}_\ell\}$, which may be determined by one of the methods below.

The bath discretization strategies developed so far in the literature are classified [43] as direct discretization (standard in the context of NRG), orthogonal polynomial representation [44,45], and numerical optimization [36,46,47]. In the present Letter we opt for the latter approach, in which the parameters $\{\gamma_\ell, \tilde{\xi}_\ell\}$ are determined by minimizing the cost function $\chi^2 = \sum_j |g(\omega_j) - \tilde{g}(\omega_j)|^2$, which is evaluated on a nonuniformly spaced grid of frequencies ω_j. To ensure a good fit of $g(\omega)$ at the subgap frequencies, we use a grid of 1000 points logarithmically spaced in the interval $\omega \in [10^{-3}\Delta, \omega_c]$, with the cutoff frequency chosen to be of the order of the largest energy scale of the problem at hand, $\omega_c \sim \max(\Delta, \Gamma, U)$. We found that a cutoff frequency $\omega_c = 10\Delta$ was appropriate in all cases analyzed below (with $D = 10\Delta$). Additional results for $D = 10^2$–$10^5\Delta$ are discussed in the Supplemental Material [48] (Refs. [49–56] are cited therein).

The exact g function (3) is shown in Fig. 2, together with the best-fit approximations $\tilde{g}(\omega)$ for $\tilde{L}\leqslant 6$, and their corresponding relative errors. We notice that by increasing $\tilde{L}$ the errors are rapidly and systematically reduced by several orders of magnitude across (and beyond) the fitting range.

Once a good fit has been found, the parameters $\{\gamma_\ell, \tilde{\xi}_\ell\}$ define the surrogate model Hamiltonian as a discretized version of Eq. (1), obtained by replacing the continuous momentum $\mathbf{k}$ by the discrete index ℓ, with $\xi_{\mathbf{k}} \to \tilde{\xi}_\ell$ and $t \to \tilde{t}_\ell$. Extending

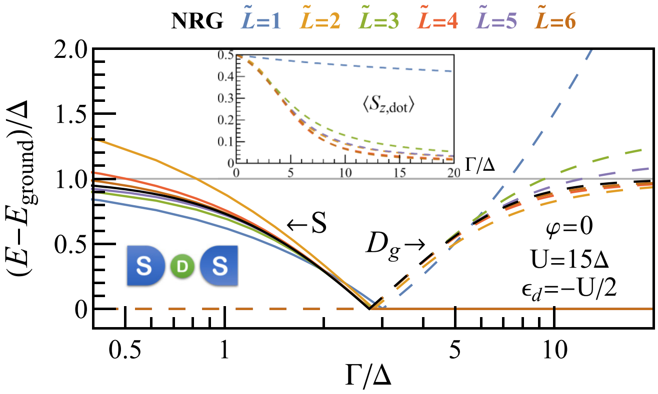

FIG. 3. SMS vs NRG [63] evolution of the subgap spectrum for an S-D-S junction with increasing coupling Γ (log scale). Continuous lines indicate the lowest singlet state S, and dashed lines indicate the gerade doublet D_g. Inset: Average spin S_z on the QD (in the D_g state) vs increasing Γ.

the model to encompass multiterminal systems with N different SC leads, this amounts to

$$\widetilde{H} = H_{\text{QD}} + \sum_{\alpha=1}^{N} (H_{\widetilde{\text{SC}},\alpha} + H_{\widetilde{\text{T}},\alpha}),$$

$$H_{\widetilde{\text{SC}},\alpha} = \sum_{\alpha\ell\sigma} \tilde{\xi}_\ell c^\dagger_{\ell\alpha\sigma} c_{\ell\alpha\sigma} - \sum_{\ell=1}^{\tilde{L}} (\Delta_\alpha e^{i\varphi_\alpha}\, c^\dagger_{\ell\alpha\uparrow} c^\dagger_{\ell\alpha\downarrow} + \text{H.c.}),$$

$$H_{\widetilde{\text{T}},\alpha} = \sum_{\ell=1}^{\tilde{L}} \sum_{\sigma=\uparrow\downarrow} \sqrt{\gamma_\ell \Gamma_\alpha} (c^\dagger_{\ell\alpha\sigma} d_\sigma + \text{H.c.}), \tag{5}$$

where $c^\dagger_{a\alpha\sigma}$ creates an electron with spin σ and energy ξ_a in the SC lead α with superconducting order parameter $\Delta_\alpha e^{i\varphi_\alpha}$. For simplicity, we restrict our attention to leads with identical gaps ($\Delta_\alpha = \Delta$), coupled with equal strength to the QD ($\Gamma_\alpha = \Gamma/N$). We solve for the low-lying eigenstates of the finite-sized effective models using exact diagonalization (ED) for $N = 1, 2$, or the density matrix renormalization group in the matrix-product-state formulation [57,58] for $N = 2, 3$. The latter is still an efficient solver for the (quasi-) one-dimensional (1D) systems considered here, and is straightforward to implement with the ITENSOR library [59,60]. The methodology described in this section constitutes the proposed surrogate model solver (SMS) for superconducting impurity problems. Our numerical codes are available online [61,62] and may be run on a standard laptop or desktop computer.

Results. First, we consider a superconductor-quantum dot-superconductor (S-D-S) junction, $N = 2$. At zero phase bias, this constitutes a single-channel problem where only the even (*gerade*) combination of quasiparticles from the two leads couple to the QD. The Γ dependence of the excitation spectrum is shown in Fig. 3 for a moderately large value of the Coulomb interaction, at the particle-hole (ph) symmetric point. While the position of the singlet-doublet quantum phase transition is rather accurately captured even by the crudest $\tilde{L} = 1$ (ZBW) approximation, deviations from the NRG data appear at higher energies in both the weak- and strong-coupling regimes.

The odd-$\tilde{L}$ surrogates always capture the correct singlet excitation energy, $E_S - E_D = \Delta$ at $\Gamma = 0$, as they contain the $\tilde{\xi}_0 = 0$ level which accommodates a screening quasiparticle with energy $E_{\text{qp}} = \Delta$. For even $\tilde{L}$, $E_{\text{qp}} > \Delta$ since all levels have $|\tilde{\xi}_\ell| > 0$, which leads to an overestimation of the singlet excitation energy. The situation at strong coupling is reversed, with even-$\tilde{L}$ surrogates performing well against the NRG data and the odd-$\tilde{L}$ ones overestimating the doublet excitation energy. This correlates with the inability of the odd-$\tilde{L}$ surrogates to properly screen the QD spin in the excited doublet (D_g), as illustrated by the inset in Fig. 3. Nevertheless, for large enough $\tilde{L}$, we obtain good convergence towards an excited doublet with a largely screened QD spin at strong coupling, in agreement with the findings of Refs. [64,65].

To gain more insight into the surrogate-model eigenstates, it is advantageous to employ the *chain* representation of our discretized SC leads where the QD only couples to the first site in each SC chain. This picture is unitarily equivalent with the *star* configuration used so far, but it offers a more geometrical perspective in the interpretation of the impurity screening process. Unlike the DMRG calculations presented in Ref. [64], however, the small surrogate model chain has no precise sense of spatial distance in the real superconductors. A detailed derivation of the star-chain mapping can be found in Appendix A of Ref. [66].

Whereas the subgap singlet state is found to have $\langle S_{z,n}\rangle = 0$ for all sites n on the chain, Fig. 4 reveals a rich spin structure of the gerade doublet (D_g) state. The inset of Fig. 4(b) shows pronounced antiferromagnetic correlations between nearest-neighbor sites of the S-D-S chain, typical to both singlet and doublet states. Qualitatively, the doublet spin structure may therefore be pictured as a delocalized $S_z = +1/2$ quasiparticle moving on top of a singlet background of antiferromagnetically correlated spins. For the one-channel problem ($\varphi = 0$) in Fig. 4(a), the extra $S_z = +1/2$ spin is preferentially distributed on the sites ferromagnetically correlated with the dot (i.e., its even-order neighbors), with a remarkable tendency of localization towards the chain boundaries (away from the dot). In odd-$\tilde{L}$ chains, the boundary sites are antiferromagnetically correlated with the dot and can only accommodate a minute fraction of the total $S_z = +1/2$ spin. The latter must then be redistributed across the entire chain (predominantly on the dot and even SC sites), thus explaining the poorly screened QD spin observed in the inset of Fig. 3. The S-D-S junction at $\varphi = \pi$ [Fig. 4(b)] features a qualitatively different spin structure, with minor differences between the spin distribution on neighboring sites; here, even the $\tilde{L} = 1$ (ZBW) approximation is qualitatively correct. Instead, the two-channel nature of the problem enables the formation of an extended spin-1/2 cloud around the impurity with negligible spin localized at the chain boundaries, visible in Fig. 4(b) for $\tilde{L} \gtrsim 5$.

Having benchmarked the SMS, we shall now illustrate its capabilities towards solving a more complex topologically nontrivial multiterminal problem. Such devices are predicted to host Weyl points in a space of synthetic dimensions defined by their superconducting phases φ_j (cf. Ref. [70] and

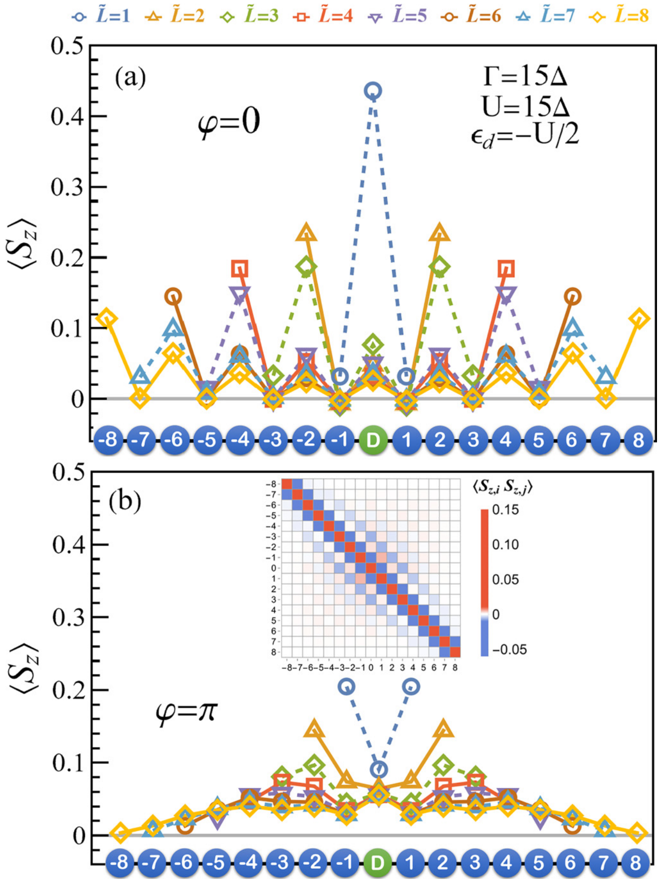

FIG. 4. Average spin $\langle S_z \rangle$ in the gerade doublet D_g state, across the chains representing the S-D-S junction at $\varphi = 0$ (a) and $\varphi = \pi$ (b), for various numbers of effective levels $\tilde{L} \leqslant 8$ per lead, obtained for $D = \omega_c = 10\Delta$. The other common parameters are $\Gamma = 15\Delta$, $U = 15\Delta$, $\epsilon_d = -U/2$. Inset in (b): Spin-spin correlation matrix $\langle S_{z,i} S_{z,j} \rangle$, $-\tilde{L} \leqslant i, j \leqslant \tilde{L}$, across the S-D-S chain at $\varphi = \pi$, where (blue) red squares indicate (antialigned) aligned spins. The spin-spin correlation matrix is qualitatively similar in both singlet and doublet states.

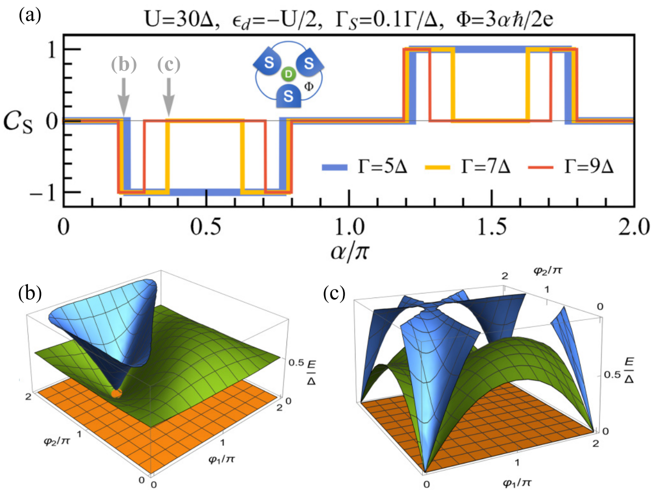

FIG. 5. Chern number and subgap spectrum in a three-terminal junction. (a) Singlet Chern number $\mathcal{C}_S$ as a function of the enclosed magnetic flux α, for various QD-SC coupling strengths Γ. (b), (c) Subgap energy spectrum near two singlet Weyl nodes, at (b) $\alpha \approx 0.21\pi$ and (c) $\alpha \approx 0.37\pi$, obtained for $\Gamma = 7\Delta$ with the $\tilde{L} = 2$ surrogate. Orange indicates the lowest (reference) singlet, blue the first excited singlet, and green the lowest doublet. For the efficient scan of the $\varphi_1 - \varphi_2$ first Brillouin zone we employed the reduced-basis method (see Supplemental Material [48] and Refs. [67–69]).

references therein). Whereas earlier theoretical predictions have been obtained exclusively in the limit of infinite superconducting gaps [70–72], the SMS allows us to explore the experimentally relevant case of finite gap and charging energy.

Here, we consider the three-terminal setup of Ref. [71] sketched in the inset of Fig. 5(a). For it to be topologically nontrivial, it is necessary to couple the SC terminals directly (we denote the corresponding tunneling rate by Γ_S), and to enclose a magnetic flux $\Phi \equiv 3\alpha\hbar/2e$. The explicit Hamiltonian may be found in the Supplemental Material [48]. A topological phase transition is signaled by a change in the Chern number, defined as the flux $\mathcal{C}(\alpha) \equiv (2\pi)^{-1} \int_0^{2\pi} \int_0^{2\pi} \mathrm{d}\varphi_1 \mathrm{d}\varphi_2 (\partial_{\varphi_1} A_2 - \partial_{\varphi_2} A_1)$ associated to the Berry connection $A_j = i\langle\psi|\partial_{\varphi_j}|\psi\rangle$ for a given (subgap) state ψ (with $\varphi_3 = 0$).

The Chern number for the lowest singlet state $\mathcal{C}_S$ (computed numerically by the method of Ref. [73]) is displayed in Fig. 5(a). Excellent convergence for this robust topological quantity was achieved already for $\tilde{L} = 2$. The results indicate that the first significant change in the system's topology appears around $\Gamma = 5\Delta$, when also tuning $\Gamma_S = 0.1\Gamma/\Delta$. Here, new pairs of singlet Weyl nodes are found to emerge at $\varphi_{1,2} = 0$, around $\alpha = (2k+1)\pi/2$, $k \in \mathbb{Z}$. They gradually and asymptotically migrate in α, with increasing coupling, towards the previously known Weyl nodes (present also in the large-gap limit), shrinking the topologically nontrivial regions in the process. The presence of local Coulomb interactions causes only small quantitative changes in the above topological phase diagram [48].

Conclusions. This Letter shows that it is possible to capture efficiently the physical properties of the impurity-induced superconducting subgap states with a model involving a very small number of effective levels, chosen to reproduce the Matsubara frequency dependence of the superconducting hybridization function. The subgap spectrum and all related observables converge rapidly and systematically to NRG and QMC results with an increasing number of levels [48].

The SMS provides easy access to the hybridization structure of the subgap states, offering insights into the doublet spin distribution and the related impurity screening process, by going beyond the limitations of the crudest ZBW and (generalized) atomic limit approaches without sacrificing the computational efficiency. Furthermore, the fast convergence of the SMS [48] enabled the solution of a fully interacting multiterminal problem, difficult to approach by means of either NRG and QMC. By its simplicity and flexibility, the SMS may prove instrumental in exploring the fully interacting many-body physics of new complex hybrid devices, which are actively being pursued for quantum information processing.

Acknowledgments. We thank R. Aguado, W. Belzig, L. Pavešić, G. Steffensen, P. Zalom, and R. Žitko for useful discussions and suggestions. This work was supported by grants of the Romanian Ministry of Education and Research, in part by Project No. PN-III-P4-ID-PCE-2020-1142, within PNCDI III, and in part by Project No. 760122/31.07.2023 within PNRR-III-C9-2022-I9. The Center for Quantum Devices is funded by the Danish National Research Foundation.

[1] L. Yu, Bound state in superconductors with paramagnetic impurities, Acta Phys. Sin. **21**, 75 (1965).
[2] H. Shiba, Classical spins in superconductors, Prog. Theor. Phys. **40**, 435 (1968).
[3] A. I. Rusinov, Superconductivity near a paramagnetic impurity, Zh. Eksp. Teor. Fiz. **9**, 146 (1968) [JETP Lett. **9**, 85 (1969)].
[4] J. Bauer, A. Oguri, and A. C. Hewson, Spectral properties of locally correlated electrons in a Bardeen–Cooper–Schrieffer, J. Phys.: Condens. Matter **19**, 486211 (2007).
[5] T. Meng, S. Florens, and P. Simon, Self-consistent description of Andreev bound states in Josephson quantum dot devices, Phys. Rev. B **79**, 224521 (2009).
[6] A. Oguri, Y. Tanaka, and J. Bauer, Interplay between Kondo and Andreev-Josephson effects in a quantum dot coupled to one normal and two superconducting leads, Phys. Rev. B **87**, 075432 (2013).
[7] G. Kiršanskas, M. Goldstein, K. Flensberg, L. I. Glazman, and J. Paaske, Yu-Shiba-Rusinov states in phase-biased superconductor-quantum dot-superconductor junctions, Phys. Rev. B **92**, 235422 (2015).
[8] M. Ruby, F. Pientka, Y. Peng, F. von Oppen, B. W. Heinrich, and K. J. Franke, Tunneling processes into localized subgap states in superconductors, Phys. Rev. Lett. **115**, 087001 (2015).
[9] M. Ruby, Y. Peng, F. von Oppen, B. W. Heinrich, and K. J. Franke, Orbital picture of Yu-Shiba-Rusinov multiplets, Phys. Rev. Lett. **117**, 186801 (2016).
[10] D.-J. Choi, C. Rubio-Verdú, J. de Bruijckere, M. M. Ugeda, N. Lorente, and J. I. Pascual, Mapping the orbital structure of impurity bound states in a superconductor, Nat. Commun. **8**, 15175 (2017).
[11] H. Huang, C. Padurariu, J. Senkpiel, R. Drost, A. L. Yeyati, J. C. Cuevas, B. Kubala, J. Ankerhold, K. Kern, and C. R. Ast, Tunnelling dynamics between superconducting bound states at the atomic limit, Nat. Phys. **16**, 1227 (2020).
[12] A. Villas, R. L. Klees, H. Huang, C. R. Ast, G. Rastelli, W. Belzig, and J. C. Cuevas, Interplay between Yu-Shiba-Rusinov states and multiple Andreev reflections, Phys. Rev. B **101**, 235445 (2020).
[13] K. Grove-Rasmussen, H. I. Jørgensen, B. M. Andersen, J. Paaske, T. S. Jespersen, J. Nygård, K. Flensberg, and P. E. Lindelof, Superconductivity-enhanced bias spectroscopy in carbon nanotube quantum dots, Phys. Rev. B **79**, 134518 (2009).
[14] R. Maurand, T. Meng, E. Bonet, S. Florens, L. Marty, and W. Wernsdorfer, First-order 0-π quantum phase transition in the kondo regime of a superconducting carbon-nanotube quantum dot, Phys. Rev. X **2**, 011009 (2012).
[15] E. J. H. Lee, X. Jiang, M. Houzet, R. Aguado, C. M. Lieber, and S. De Franceschi, Spin-resolved Andreev levels and parity crossings in hybrid superconductor–semiconductor nanostructures, Nat. Nanotechnol. **9**, 79 (2014).
[16] A. Jellinggaard, K. Grove-Rasmussen, M. H. Madsen, and J. Nygård, Tuning Yu-Shiba-Rusinov states in a quantum dot, Phys. Rev. B **94**, 064520 (2016).
[17] R. Delagrange, R. Weil, A. Kasumov, M. Ferrier, H. Bouchiat, and R. Deblock, 0-π quantum transition in a carbon nanotube Josephson junction: Universal phase dependence and orbital degeneracy, Phys. B: Condens. Matter **536**, 211 (2018).
[18] G. O. Steffensen, J. C. Estrada Saldaña, A. Vekris, P. Krogstrup, K. Grove-Rasmussen, J. Nygård, A. L. Yeyati, and J. Paaske, Direct transport between superconducting subgap states in a double quantum dot, Phys. Rev. B **105**, L161302 (2022).
[19] A. Bargerbos, M. Pita-Vidal, R. Žitko, J. Ávila, L. J. Splitthoff, L. Grünhaupt, J. J. Wesdorp, C. K. Andersen, Y. Liu, L. P. Kouwenhoven, R. Aguado, A. Kou, and B. van Heck, Singlet-doublet transitions of a quantum dot Josephson junction detected in a transmon circuit, PRX Quantum **3**, 030311 (2022).
[20] V. Fatemi, P. D. Kurilovich, M. Hays, D. Bouman, T. Connolly, S. Diamond, N. E. Frattini, V. D. Kurilovich, P. Krogstrup, J. Nygård, A. Geresdi, L. I. Glazman, and M. H. Devoret, Microwave susceptibility observation of interacting many-body andreev states, Phys. Rev. Lett. **129**, 227701 (2022).
[21] M. Pita-Vidal, A. Bargerbos, R. Žitko, L. J. Splitthoff, L. Grünhaupt, J. J. Wesdorp, Y. Liu, L. P. Kouwenhoven, R. Aguado, B. van Heck, A. Kou, and C. K. Andersen, Direct manipulation of a superconducting spin qubit strongly coupled to a transmon qubit, Nat. Phys. **19**, 1110 (2023).
[22] A. Mishra, P. Simon, T. Hyart, and M. Trif, Yu-Shiba-Rusinov qubit, PRX Quantum **2**, 040347 (2021).
[23] L. Pavešić and R. Žitko, Qubit based on spin-singlet Yu-Shiba-Rusinov states, Phys. Rev. B **105**, 075129 (2022).
[24] T. Dvir, G. Wang, N. van Loo, C.-X. Liu, G. P. Mazur, A. Bordin, S. L. D. Ten Haaf, J.-Y. Wang, D. van Driel, F. Zatelli, X. Li, F. K. Malinowski, S. Gazibegovic, G. Badawy, E. P. A. M. Bakkers, M. Wimmer, and L. P. Kouwenhoven, Realization of a minimal Kitaev chain in coupled quantum dots, Nature (London) **614**, 445 (2023).
[25] A. Martín-Rodero and A. L. Yeyati, Josephson and Andreev transport through quantum dots, Adv. Phys. **60**, 899 (2011).
[26] V. Meden, The Anderson–Josephson quantum dot—A theory perspective, J. Phys.: Condens. Matter **31**, 163001 (2019).
[27] P. Zalom, Rigorous Wilsonian renormalization group for impurity models with a spectral gap, arXiv:2307.07479.
[28] V. Pokorný and M. Žonda, Effective low-energy models for superconducting impurity systems, Phys. Rev. B **107**, 155111 (2023).
[29] C. Hermansen, A. L. Yeyati, and J. Paaske, Inductive microwave response of Yu-Shiba-Rusinov states, Phys. Rev. B **105**, 054503 (2022).
[30] A. V. Rozhkov and D. P. Arovas, Interacting-impurity Josephson junction: Variational wave functions and slave-boson mean-field theory, Phys. Rev. B **62**, 6687 (2000).
[31] M. Žonda, P. Zalom, T. Novotný, G. Loukeris, J. Bätge, and V. Pokorný, Generalized atomic limit of a double quantum dot coupled to superconducting leads, Phys. Rev. B **107**, 115407 (2023).
[32] E. Vecino, A. Martín-Rodero, and A. Levy Yeyati, Josephson current through a correlated quantum level: Andreev states and π junction behavior, Phys. Rev. B **68**, 035105 (2003).
[33] K. Grove-Rasmussen, G. Steffensen, A. Jellinggaard, M. H. Madsen, R. Žitko, J. Paaske, and J. Nygård, Yu–Shiba–Rusinov

screening of spins in double quantum dots, Nat. Commun. **9**, 2376 (2018).

[34] J. Kondo, Resistance minimum in dilute magnetic alloys, Prog. Theor. Phys. **32**, 37 (1964).

[35] A. Georges, G. Kotliar, W. Krauth, and M. J. Rozenberg, Dynamical mean-field theory of strongly correlated fermion systems and the limit of infinite dimensions, Rev. Mod. Phys. **68**, 13 (1996).

[36] M. Caffarel and W. Krauth, Exact diagonalization approach to correlated fermions in infinite dimensions: Mott transition and superconductivity, Phys. Rev. Lett. **72**, 1545 (1994).

[37] E. Koch, G. Sangiovanni, and O. Gunnarsson, Sum rules and bath parametrization for quantum cluster theories, Phys. Rev. B **78**, 115102 (2008).

[38] A. Liebsch and H. Ishida, Temperature and bath size in exact diagonalization dynamical mean field theory, J. Phys.: Condens. Matter **24**, 053201 (2012).

[39] C. Mejuto-Zaera, L. Zepeda-Núñez, M. Lindsey, N. Tubman, B. Whaley, and L. Lin, Efficient hybridization fitting for dynamical mean-field theory via semi-definite relaxation, Phys. Rev. B **101**, 035143 (2020).

[40] M. Granath and H. U. R. Strand, Distributional exact diagonalization formalism for quantum impurity models, Phys. Rev. B **86**, 115111 (2012).

[41] M. Granath and J. Schött, Signatures of coherent electronic quasiparticles in the paramagnetic Mott insulator, Phys. Rev. B **90**, 235129 (2014).

[42] S. Motahari, R. Requist, and D. Jacob, Kondo physics of the Anderson impurity model by distributional exact diagonalization, Phys. Rev. B **94**, 235133 (2016).

[43] I. de Vega, U. Schollwöck, and F. A. Wolf, How to discretize a quantum bath for real-time evolution, Phys. Rev. B **92**, 155126 (2015).

[44] R. S. Burkey and C. D. Cantrell, Discretization in the quasi-continuum, J. Opt. Soc. Am. B **1**, 169 (1984).

[45] L. Boehnke, H. Hafermann, M. Ferrero, F. Lechermann, and O. Parcollet, Orthogonal polynomial representation of imaginary-time Green's functions, Phys. Rev. B **84**, 075145 (2011).

[46] C. Gramsch, K. Balzer, M. Eckstein, and M. Kollar, Hamiltonian-based impurity solver for nonequilibrium dynamical mean-field theory, Phys. Rev. B **88**, 235106 (2013).

[47] A. Dorda, M. Nuss, W. von der Linden, and E. Arrigoni, Auxiliary master equation approach to nonequilibrium correlated impurities, Phys. Rev. B **89**, 165105 (2014).

[48] See Supplemental Material at http://link.aps.org/supplemental/10.1103/PhysRevB.108.L220506 for more information on the hybridization function fitting procedure, effective one-channel surrogate models for multichannel problems, reduced basis methodology, technical details on the three-terminal junction modeling, and additional surrogate model benchmarks against NRG and QMC.

[49] Wolfram Inc., Mathematica, version 12.3, https://www.wolfram.com/mathematica/ (2021).

[50] R. Zitko, Josephson potentials for single impurity Anderson impurity in a junction between two superconductors, https://doi.org/10.5281/zenodo.5874832 (2022).

[51] R. Zitko, NRG Ljubljana, https://doi.org/10.5281/zenodo.4841076 (2021).

[52] M. Žonda, V. Pokorný, V. Janiš, and T. Novotný, Perturbation theory for an Anderson quantum dot asymmetrically attached to two superconducting leads, Phys. Rev. B **93**, 024523 (2016).

[53] C. Karrasch, A. Oguri, and V. Meden, Josephson current through a single Anderson impurity coupled to BCS leads, Phys. Rev. B **77**, 024517 (2008).

[54] Y. Tanaka, A. Oguri, and A. C. Hewson, Kondo effect in asymmetric Josephson couplings through a quantum dot, New J. Phys. **9**, 115 (2007).

[55] P. Zalom, V. Pokorný, and T. Novotný, Spectral and transport properties of a half-filled Anderson impurity coupled to phase-biased superconducting and metallic leads, Phys. Rev. B **103**, 035419 (2021).

[56] P. Zalom and T. Novotný, Tunable reentrant Kondo effect in quantum dots coupled to metal-superconducting hybrid reservoirs, Phys. Rev. B **104**, 035437 (2021).

[57] S. R. White, Density matrix formulation for quantum renormalization groups, Phys. Rev. Lett. **69**, 2863 (1992).

[58] U. Schollwöck, The density-matrix renormalization group in the age of matrix product states, Ann. Phys. **326**, 96 (2011).

[59] M. Fishman, S. R. White, and E. M. Stoudenmire, The ITensor software library for tensor network calculations, SciPost Phys. Codebases **4** (2022).

[60] M. Fishman, S. R. White, and E. M. Stoudenmire, Codebase release 0.3 for ITensor, SciPost Phys. Codebases **4-r0.3** (2022).

[61] E. J. P. Frost, FermPy (exact diagonalization) GitHub repository, https://github.com/emilfrost/fermpy (2023).

[62] V. V. Baran, Surrogate models GitHub repository, https://github.com/virgilb91/surrogate_models/tree/main (2023).

[63] We are grateful to P. Zalom for providing us with the results of the NRG Ljubljana implementation. The one-channel NRG implementation has then been employed at $D = 10\Delta$, $\Lambda = 2$ with 500 kept states and no z averaging.

[64] C. P. Moca, I. Weymann, M. A. Werner, and G. Zaránd, Kondo cloud in a superconductor, Phys. Rev. Lett. **127**, 186804 (2021).

[65] L. Pavešič, R. Aguado, and R. Žitko, Quantum dot Josephson junctions in the strong-coupling limit, arXiv:2304.12456.

[66] R. Bulla, H.-J. Lee, N.-H. Tong, and M. Vojta, Numerical renormalization group for quantum impurities in a bosonic bath, Phys. Rev. B **71**, 045122 (2005).

[67] V. V. Baran and D. R. Nichita, Reduced basis emulation of pairing in finite systems, Phys. Rev. B **107**, 144503 (2023).

[68] M. F. Herbst, B. Stamm, S. Wessel, and M. Rizzi, Surrogate models for quantum spin systems based on reduced-order modeling, Phys. Rev. E **105**, 045303 (2022).

[69] P. Brehmer, M. F. Herbst, S. Wessel, M. Rizzi, and B. Stamm, Reduced basis surrogates for quantum spin systems based on tensor networks, Phys. Rev. E **108**, 025306 (2023).

[70] L. Teshler, H. Weisbrich, J. Sturm, R. L. Klees, G. Rastelli, and W. Belzig, Ground state topology of a four-terminal superconducting double quantum dot, SciPost Phys. **15**, 214 (2023).

[71] R. L. Klees, G. Rastelli, J. C. Cuevas, and W. Belzig, Microwave spectroscopy reveals the quantum geometric tensor of topological Josephson matter, Phys. Rev. Lett. **124**, 197002 (2020).

[72] R. L. Klees, J. C. Cuevas, W. Belzig, and G. Rastelli, Ground-state quantum geometry in superconductor–quantum dot chains, Phys. Rev. B **103**, 014516 (2021).

[73] T. Fukui, Y. Hatsugai, and H. Suzuki, Chern numbers in discretized Brillouin zone: Efficient method of computing (spin) Hall conductances, J. Phys. Soc. Jpn. **74**, 1674 (2005).